NJC

PAPER

View Article Online
View Journal | View Issue

Cite this: *New J. Chem.*, 2014, **38**, 529

Carbohydrates in the gas phase: conformational preference of D-ribose and 2-deoxy-D-ribose†

Luis Miguel Azofra,*[a] María Mar Quesada-Moreno,[b] Ibon Alkorta,[a] Juan Ramón Avilés-Moreno,[b] Juan Jesús López-González[b] and José Elguero[a]

Received (in Montpellier, France) 10th September 2013, Accepted 1st November 2013

DOI: 10.1039/c3nj01076g

www.rsc.org/njc

A full exploration of the conformational landscape of D-ribose and 2-deoxy-D-ribose monosaccharides in the gas phase has been performed using DFT methods (B3LYP and M06-2X). Open-chain, furanose and pyranose configurations have been examined. Up to 954 and 668 stable structures have been obtained for D-ribose and 2-deoxy-D-ribose. Among these structures, up to 35 and 22 have relative energies smaller than 5 kJ mol^{-1} with respect to the absolute minimum of each molecule, respectively. For D-ribose, pyranose in α- and β-forms is the most populated according to both functionals, the β-diastereoisomer being the most populated. For 2-deoxy-D-ribose, the α-pyranose form is in majority. The β/α relationship of pyranose forms presents different results for both functionals: for M06-2X it increases in D-ribose and decreases in 2-deoxy-D-ribose at 0 K with respect to the room temperature results, the opposite case occurring in B3LYP. Intramolecular weak interactions have been characterized using the AIM and NBO methodologies.

Introduction

Carbohydrates are important molecules since they are the most abundant organic compounds on Earth by mass showing a large number of functions, as energy storage molecules, building blocks, as well as bacterial and viral recognition targets.[1] Amongst them, oligosaccharides have important medical applications such as the influenza virus treatment (Tamiflu, Heparin and different kinds of vaccines).[2] The anomeric effect continues to be a subject of recent studies,[3,4] as well as the conformational aspects of carbohydrates,[5] in particular free fructose and furanose oligosaccharides.[6,7] Besides, D-ribose and 2-deoxy-D-ribose are constituents of the nucleic acids RNA and DNA, respectively.

The importance of the study of carbohydrates in the gas phase resides in the recent detection of prebiotic building blocks, highly relevant in biology and astrochemistry[8,9] because these blocks could be involved in the construction of more complex molecules for the emergence of life. For example, the smaller sugars, with two[10,11] and three[11–15] carbon atoms, have been found in the interstellar space (interstellar SgrB2 cloud) and in the Murchinson meteorite.

D-Ribose is an aldopentose ($C_5H_{10}O_5$) which can exist in five forms: one linear, the open-chain configuration, and four cyclic, two furanose forms (five-membered ring; α- and β-) and two pyranose ones (six-membered ring; α- and β-). 2-Deoxy-D-ribose ($C_5H_{10}O_4$) is a reduced derivative of D-ribose which has no hydroxyl group on C2 (see Fig. 1).

The literature for D-ribose is large. Different studies have been reported in solid, solution and gas phases. In 2010, Šišak and co-workers[16] found β/α-pyranose ratios of 2 : 1 and 3 : 1 for the powder and single-crystal, respectively, using NMR spectroscopy and X-ray diffraction techniques. Concerning D-ribose in solution, Lemieux *et al.*[17] reported approximate percentage ratios of 43(βp) : 42(αp) : 10(βf) : 5(αf) at 0 °C and 30(βp) : 30(αp) : 18(βf) : 22(αf) at 90 °C using ^{1}H NMR spectroscopy and OR (optical rotatory) measurements in the study of its mutarotation in H_2O and D_2O. Finally, Cocinero and co-workers[18] published in 2012 an article in which they studied, experimentally and theoretically, D-ribose in the gas phase. Their MP2 results offer percentage ratios of 63.8(βp) : 35.8(αp) : 0.35(βf) : 0.04(αf) : 0.00(linear) while experimentally they are 65.4(βp) : 32.5(αp). In addition, it is noteworthy that there is a lack of structural information for 2-deoxy-D-ribose.

In this work, we present a full exploration of the conformational landscape of D-ribose and 2-deoxy-D-ribose monosaccharides in the gas phase using DFT (B3LYP and M06-2X) methods in order to predict the most stable conformers of the above mentioned carbohydrates. Also, the role of the intramolecular weak interactions in the monosaccharides has been the target of a comprehensive study establishing relationships

[a] *Instituto de Química Médica (C.S.I.C.), Juan de la Cierva, 3, E-28006 Madrid, Spain. E-mail: luisazofra@iqm.csic.es; Web: http://are.iqm.csic.es/; Fax: +34 91 564 48 53*

[b] *Department of Physical and Analytical Chemistry, University of Jaén, Campus Las Lagunillas, E-23071 Jaén, Spain*

† Electronic supplementary information (ESI) available. See DOI: 10.1039/c3nj01076g

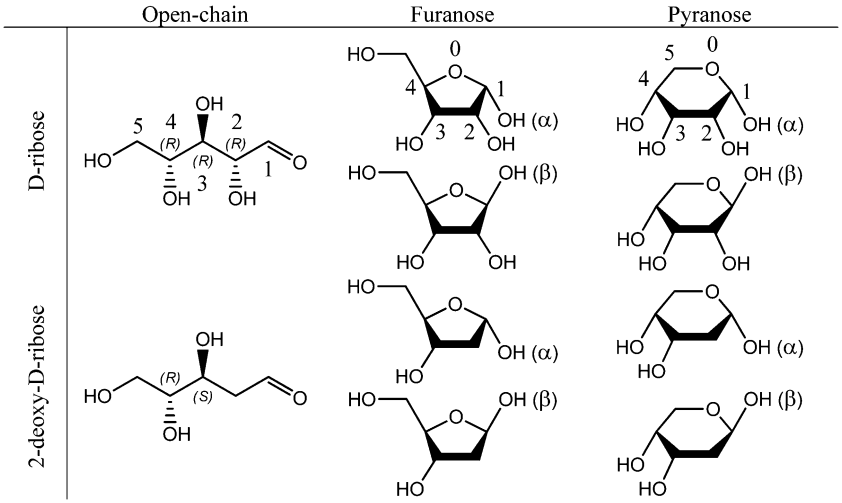

Fig. 1 Left to right and top to bottom: open-chain, furanose and pyranose configurations of D-ribose and 2-deoxy-D-ribose. The orientation of the hydroxyl group on the anomeric carbon atom (C1) in the cyclic forms gives the α- (*exo* face) and β- (*endo* face) diastereoisomers. The absolute configuration of the stereogenic centers is indicated in the linear forms. The numbering labeling in the D-ribose structures (extends to 2-deoxy-D-ribose) follows the IUPAC recommendations.

based on the electron density descriptors and orbital interaction energy for both sugars.

Computational methods

The conformational explorations were conducted in two steps. In the first one, a large number of initial structures was chosen based on the different rotatable bonds. In the open-chain configurations, three initial structures were considered for each of them (*gauche*, *g*, *gauche′*, *g′*, and *trans*, *t*, conformations). Thus, 2187 ($=3^7$) and 6561 ($=3^8$) were considered for the open-chain configuration of the 2-deoxy-D-ribose and D-ribose, respectively. In the furanose configuration, twenty limit ring conformations (ten envelope and ten twist) were taken into account and three structures for each rotatable bond not belonging to the ring, which makes 1620 ($=20 \times 3^4$) and 4860 ($=20 \times 3^5$) initial structures for the 2-deoxy-D-ribose and D-ribose, respectively. Finally, in the pyranose configuration, thirty eight limit ring conformations (two chair, twelve half-chair, six skew, six boat and twelve envelope) which accounts for a total of 1026 ($=38 \times 3^3$) and 3078 ($=38 \times 3^4$) initial structures for the 2-deoxy-D-ribose and D-ribose, respectively. All these initial structures were optimized in the vacuum with the Becke,[19] three-parameter, Lee–Yang–Parr[20] density functional (B3LYP) and Pople's basis set 6-31G.[21] Subsequently, all the structures were compared in order to eliminate those which are duplicated. The simultaneous fulfillment of two screening criteria, geometrical root mean square (rms) smaller than 0.05 Å and electronic energy differences less than 0.1 kJ mol^{-1}, was used to consider two structures identical.[22] In the second step, the resulting geometries were re-optimized in the gas phase with two functionals, the M06-2X[23] and the B3LYP,[19,20] in both cases with the Pople's 6-311++G(d,p) basis set[21] which includes diffuse and polarization functions for heavy and hydrogen atoms. M06-2X has been proven to be a good functional for descriptive purposes[24,25] with a relatively low computational cost.[26] The screening criteria were also applied to all these new structures. Finally, frequency calculations were carried out for the unique structures in order to confirm that they correspond to real minima and to obtain the value of the Zero Point Energy (ZPE). The electronic energies were corrected with the ZPE.

All the DFT-calculations were carried out with the GAUSSIAN09 package.[27] Furthermore, the ring puckering analysis methodology developed by Cremer and Pople[28] was applied in order to characterize the pseudorotation P, θ and ϕ parameters. Those parameters overlaid on the Altona–Sundaralingam wheel-sphere[29] provide the ring conformation type, as well as the Q amplitude, that is, how much the ring is distorted with respect to the planar case. For this purpose, the RING96[28,30] and some in-house programs were employed.[22]

Moreover, the electron density of the systems was analyzed with the Atoms in Molecules (AIM) methodology[31,32] using the MORPHY[33–35] and the AIMAll[36] programs. On the basis of this methodology, the presence of bond critical points (BCP) and the values of their electron density and their Laplacian provide information on the covalent and weak interactions present in the molecules.[31,37,38] Also, ring critical points (RCP) and cage critical points (CCP) give a significant idea about the topological structure. Finally, the Natural Bond Orbital (NBO) theory[39] was applied for the orbital characterization of the weak interactions. These calculations were carried out with the NBO3.1 program[40] implemented in the GAUSSIAN09 program.

Results and discussion

This section has been divided into two parts. In the first one, the structure, topology and energy of the most stable minima in the gas phase will be discussed. In the second one, a complete study of the intramolecular weak interactions will be done based on two different approaches: (i) topology of the

electron density, through the principles offered by the AIM theory and (ii) orbital, using the NBO methodology. Furthermore, both results will be compared and discussed.

Along the exposition of this section, a set of abbreviations will be used. Thus dDR, dDRαf, dDRβf, dDRαp, and dDRβp correspond to open-chain 2-deoxy-D-ribose, α-2-deoxy-D-ribofuranose, β-2-deoxy-D-ribofuranose, α-2-deoxy-D-ribopyranose, and β-2-deoxy-D-ribopyranose. In the same way, DR, DRαf, DRβf, DRαp and DRβp refer to open-chain D-ribose, α-D-ribofuranose, β-D-ribofuranose, α-D-ribopyranose and β-D-ribopyranose, respectively.

1. Structures, topology and energies

The number of unique minima, obtained in the conformational searches of 2-deoxy-D-ribose and D-ribose using two functionals, M06-2X and B3LYP, is gathered in Table 1. Also, the number of the most stable minima (with relative energy less than 5 kJ mol^{-1}) is shown in Table 1. In both cases, similar values were obtained for the two DFT methods. Due to the restrictions imposed by the ring, the number of minima obtained in the cyclic configurations is much smaller (up to 82) than in the open-chain forms (up to 650). Fig. 2 shows the energy ranking at the M06-2X/6-311++G(d,p) computational level; all these minima span in the open-chain 2-deoxy-D-ribose and D-ribose configurations over a range of 58 and 68 kJ mol^{-1}, respectively. These limits decrease for the furanose configurations to ranges of 42, 34, 50 and 48 kJ mol^{-1} for α-2-deoxy-D-ribofuranose, β-2-deoxy-D-ribofuranose, α-D-ribofuranose and β-D-ribofuranose, respectively. For the pyranose configurations, the range increases for α-2-deoxy-D-ribopyranose and decreases for β-2-deoxy-D-ribopyranose, the same range occurring for β-D-ribopyranose and α-D-ribopyranose, with 61, 52, 77 and 60 kJ mol^{-1}, respectively. All the ranking profiles exhibit a common profile: in the borders (the most stable and unstable minima) the growth is more pronounced, being smoother in the middle zone, especially in the linear forms. The exception occurs for the α-2-deoxy-D-ribofuranose with a practical linear trend in the whole plot, Fig. 2(b).

Table 1 Number of unique minima for the different conformers of 2-deoxy-D-ribose and D-ribose and number of their most stable ones (with relative energy less than 5 kJ mol^{-1})

	B3LYP		M06-2X	
Structure	Total	<5 kJ mol^{-1}	Total	<5 kJ mol^{-1}
Open-chain 2-deoxy-D-ribose	450	3	445	3
Open-chain D-ribose	639	7	650	9
α-2-Deoxy-D-ribofuranose	55	3	59	2
β-2-Deoxy-D-ribofuranose	64	10	66	4
α-D-Ribofuranose	69	9	72	5
β-D-Ribofuranose	74	10	82	10
α-2-Deoxy-D-ribopyranose	46	1	46	1
β-2-Deoxy-D-ribopyranose	53	5	51	3
α-D-Ribopyranose	72	5	73	4
β-D-Ribopyranose	74	4	77	4

The number of minima found in D-ribose and 2-deoxy-D-ribose is larger than in other any study previously reported for these molecules. The evaluation of a complete set of initial structures is fundamental in order to obtain the full exploration of the PES (Potential Energy Surface).

The molecular graphs of the most stable minima (less than 3 kJ mol^{-1}) for the open-chain, furanose and pyranose conformers calculated at the M06-2X/6-311++G(d,p) computational level are shown in Fig. 3–5, respectively. Also, in Fig. S1 of the ESI,† are gathered the electron density molecular graphs of the most stable minima with relative energy less than 5 kJ mol^{-1}. The open-chain 2-deoxy-D-ribose presents 3 minima with relative energy less than 5 kJ mol^{-1}. The most stable minimum presents a *tt* conformation, while in the second one (E_{rel} = 2.8 kJ mol^{-1}), the carbon skeleton shows *gg′* dihedral angles. This compact structure had been characterized in the literature as a reactive form in the intramolecular hemiacetal formation leading to a pyranose structure.[41] The existence of a hydrogen bond (HB) between the hydroxyl group located on C5 and the oxygen atom of the aldehyde group stabilizes this configuration. Also, this second most stable minimum exhibits a non-expected topology with the appearance of two RCP, and therefore, a CCP between them.

The open-chain D-ribose has a total of 9 minima with relative energies less than 5 kJ mol^{-1}. Most of these minima show at least one of the dihedral angles of the carbon skeleton with a *t* conformation, with the first compact structure (*gg*) in the sixth ranking position (E_{rel} = 3.2 kJ mol^{-1}). It shows a HB between the hydroxyl groups on C2 and C4 and one O···C interaction between the hydroxyl group on the C2 and the C4 atom. This interaction type is characterized by a curved bond path which

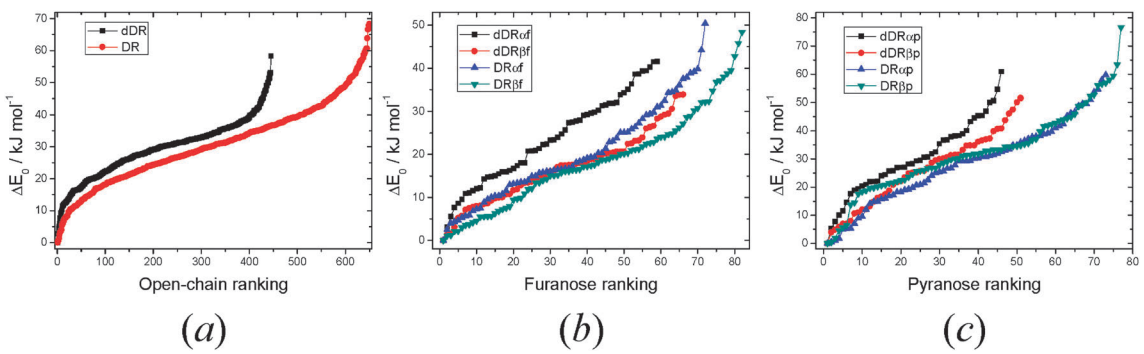

Fig. 2 Energy ranking of the (a) open-chain; (b) furanose; and (c) pyranose configuration minima calculated at the M06-2X/6-311++G(d,p) computational level.

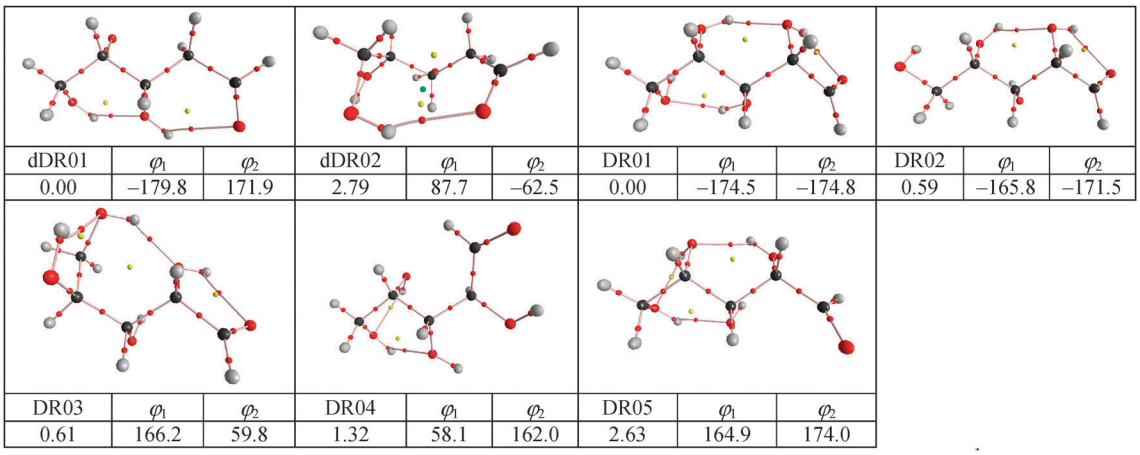

Fig. 3 Molecular graphs of the most stable conformers (less than 3 kJ mol^{-1}) for the open-chain forms of 2-deoxy-D-ribose and D-ribose in the gas phase calculated at the M06-2X/6-311++G(d,p) computational level. For linear forms, dihedral angles $D_{C1C2C3C4}$ (φ_1) and $D_{C2C3C4C5}$ (φ_2) in degrees are shown. Small points are BCP (red), RCP (yellow) and CCP (green).

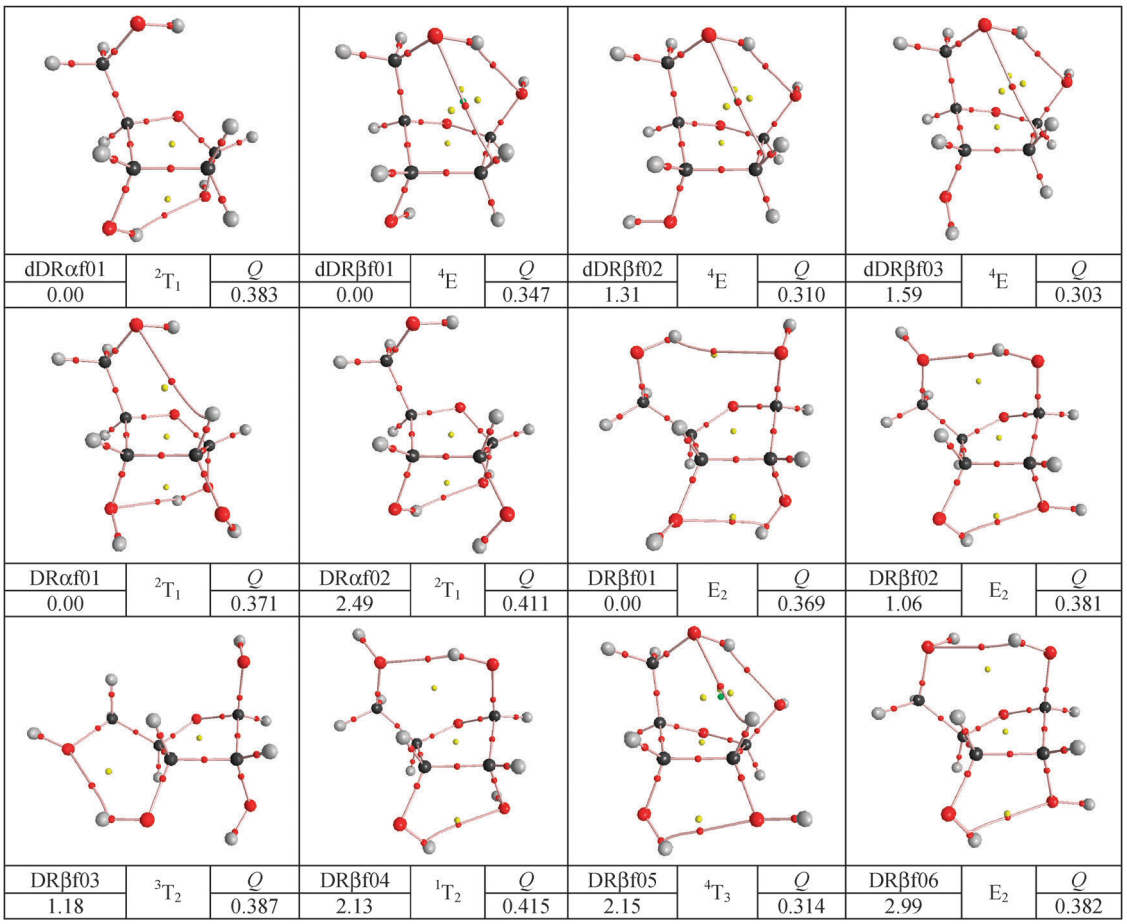

Fig. 4 Molecular graphs of the most stable conformers (less than 3 kJ mol^{-1}) for the furanose forms of 2-deoxy-D-ribose and D-ribose in the gas phase calculated at the M06-2X/6-311++G(d,p) computational level. The ring conformation, as well as the *Q* parameter in Å, are included. Relative energies are in kJ mol^{-1}. Small points are BCP (red), RCP (yellow) and CCP (green). T = twist and E = envelope. Superscript on the left refers to *endo* face. Subscript on the right refers to *exo* face.

starts in the oxygen atom nuclear attractor and, in vicinity of the BCP, strongly deviates from the carbon atom nuclear attractor. This topological entity is associated with a weak potential HB. Specifically, the ninth most stable minimum (E_{rel} = 3.9 kJ mol^{-1}) presents a *gt* conformation and an interaction between the hydroxyl group on C4 and the sp^2 carbon atom which can be

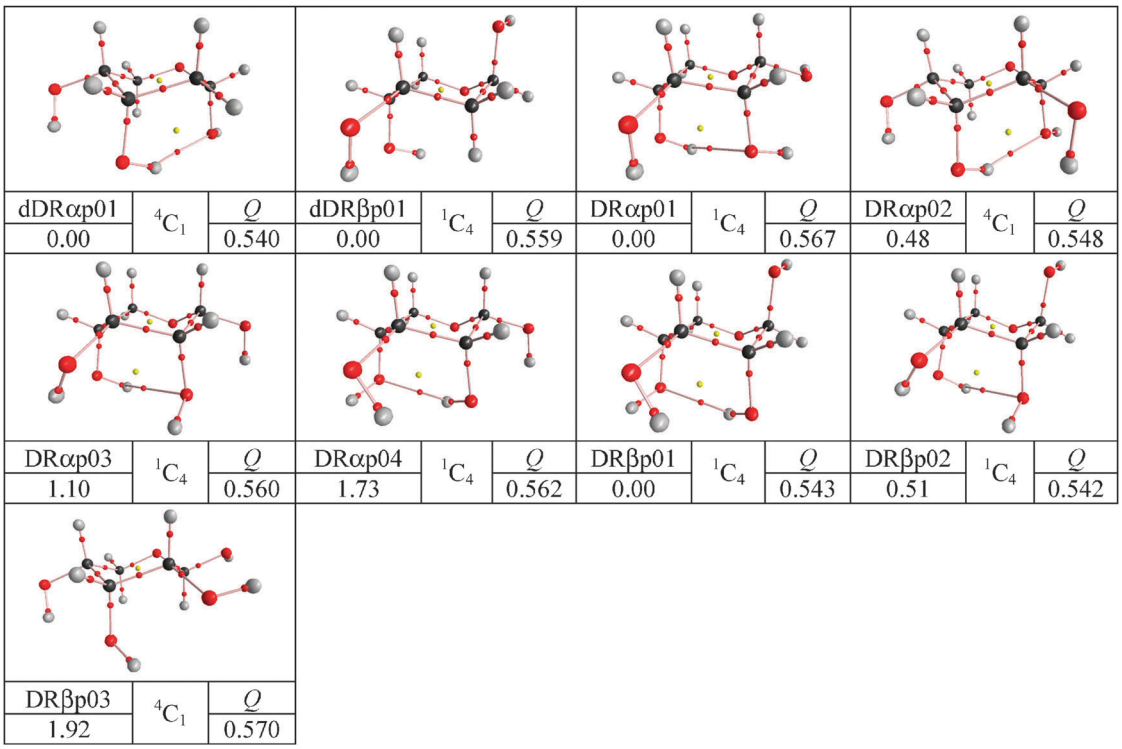

Fig. 5 Molecular graphs of the most stable conformers (less than 3 kJ mol^{-1}) for the pyranose forms of 2-deoxy-D-ribose and D-ribose in the gas phase calculated at the M06-2X/6-311++G(d,p) computational level. The ring conformation, as well as the *Q* parameter in Å are included. Relative energies are in kJ mol^{-1}. Small points are BCP (red), RCP (yellow) and CCP (green). C = chair, H = half-chair, S = skew, B = boat, T = twist and E = envelope. Superscript on the left refers to the *endo* face. Subscript on the right refers to the *exo* face.

considered as the precursor structure to the furanose formation. A similar interaction has been recently described in the salicylic acid.[42]

In α- and β-2-deoxy-D-ribofuranose the number of minima with relative energy less than 5 kJ mol^{-1} is 2 and 5, respectively. For the α-diastereoisomer, the first and second most stable minima (E_{rel} = 3.1 kJ mol^{-1}) present $^{2}T_{1}$ and ^{2}E ring conformations, respectively. These two conformations are very similar as indicated by their proximity in the Altona–Sundaralingam wheel,[29] presenting a HB between the hydroxyl groups in the *exo* face, in both cases. For the β-diastereoisomer, the first three most stable minima (E_{rel} = 1.3 and 1.6 kJ mol^{-1}) exhibit a ^{4}E ring conformation which facilitates the HB between the hydroxyl moiety on C1 and the hydroxyl group of the hydroxymethyl ones in the *endo* face, and also, an O···C interaction similar to the one previously discussed. The fourth most stable structure (E_{rel} = 3.1 kJ mol^{-1}) with an E_{2} ring conformation presents a long HB (2.29 Å) in the *endo* face but not an O···C interaction since the hydroxymethyl group is situated far away from the C2 atom.

In the α- and β-D-ribofuranoses, the number of most stable minima is 5 and 10, respectively. The α-diastereoisomer has a $^{2}T_{1}$ ring conformation for the first and second most stable minima (E_{rel} = 2.5 kJ mol^{-1}) and the proximal ^{2}E for the fourth and fifth most stable ones (E_{rel} = 4.3 and 4.7 kJ mol^{-1}). These four conformations show a HB between the hydroxyl groups on C1 and C3 in the *exo* face. In addition, a CH···O HB between the C2H moiety and the oxygen of the hydroxymethyl group is observed in the first and fifth most stable minima. The third most stable minimum (E_{rel} = 4.0 kJ mol^{-1}), which has a $^{3}T_{4}$ ring conformation, exhibits a chain of HBs between the hydroxyl groups on C3, C2 and C1.

The minima of the β-diastereoisomer can be divided into three groups: (i) the first, second, fourth, sixth and eighth most stable minima have E_{2} or $^{1}T_{2}$ ring conformations which allow the HB formation between the hydroxyl moieties in the *exo* face and the two hydroxyl groups in the *endo* face, except for the last minimum; (ii) the third and seventh most stable minima are in $^{3}T_{2}$ ring conformation. In the third most stable minimum there is a HB between the hydroxymethyl group and the hydroxyl one on C3, *i.e.*, between moieties located in different faces due to the conformational freedom of the –CH_2OH group; and (iii) the fifth and tenth most stable minima with $^{4}T_{3}$ and ^{4}E ring conformations, respectively, showed the two HBs described in case (i), and additionally the HB between the hydroxymethyl moiety and the alkyl hydrogen atom on C2.

Finally, the number of minima with relative energy less than 5 kJ mol^{-1} for α-2-deoxy-D-ribopyranose, β-2-deoxy-D-ribopyranose, α-D-ribopyranose and β-D-ribopyranose is 1, 3, 4 and 4, respectively. One of the most important characteristics of these conformers is that all of them exhibit chair conformations of the ring ($^{1}C_{4}$ or $^{4}C_{1}$). For instance, the most stable conformer with a non-chair conformation for the α-2-deoxy-D-ribopyranose has a skew $^{1}S_{5}$ ring conformation, and it appears in the tenth

ranking position with a relative energy of 9.8 kJ mol^{-1}. $^1C_4$ conformation of D-ribose presents HB interactions between the hydroxyl groups on C2 and C4, and $^4C_1$, both D-ribose and 2-deoxy-D-ribose, between C1 and C3. Only in the case of the β-2-deoxy-D-ribopyranose no intramolecular weak interactions have been found.

Table S1 of the ESI† reports the relative energies of the most stable minima (less than 5 kJ mol^{-1}) at the M06-2X/6-311++G(d,p) computational level. In addition, a comparison with the B3LYP results is offered. The numbering is referenced to the M06-2X minima energies; thus, it is possible to compare alike structures with the two functionals used here. In all the cases, the most stable structure is the same with the two functionals (M06-2X and B3LYP), with the exception of the α-D-ribofuranose and β-D-ribopyranose since in B3LYP it is the second most stable one. In general, the classification is similar in the open-chain and pyranose forms, but not for the furanose ones.

The Boltzmann populations, in percentage, for D-ribose and 2-deoxy-D-ribose at the B3LYP and M06-2X DFT-levels of theory are gathered in Table 2. At room temperature (T = 298.16 K), for D-ribose: (i) both functionals provide a majority of pyranose (α- and β-) forms; (ii) the relative ratio of β/α-pyranose is estimated to be 1.6 : 1 and 1.2 : 1 for B3LYP and M06-2X, respectively; and (iii) B3LYP provides populations of 8.2, 3.4 and 0.6% for open-chain, α-furanose and β-furanose forms, while for M06-2X they are 0.0, 0.2 and 0.0%. For 2-deoxy-D-ribose: (i) a majority of α-pyranose form has been obtained but with a 58.4% in B3LYP and a 88.2% in M06-2X; (ii) similar quantities are obtained for β-pyranose forms: 13.8 and 10.9% for B3LYP and M06-2X, respectively; and (iii) B3LYP provides higher populations of open-chain forms, 20.4%, while for M06-2X it is 0.0%. At 0 K, similar values have been obtained for D-ribose and 2-deoxy-D-ribose using the M06-2X functional. The main feature to note is the decrease of α-pyranose and the increase of β-pyranose populations in D-ribose with respect to the room temperature, so that, the β/α ratio in pyranose forms increases at 0 K. The opposite case occurs in 2-deoxy-D-ribose. Prominent differences are observed in the B3LYP results. In D-ribose, the presence of open-chain forms goes practically to zero and both pyranose anomers increase their populations.

Table 2 Boltzmann populations[a] in percentage for D-ribose and 2-deoxy-D-ribose at B3LYP/6-311++G(d,p) and M06-2X/6-311++G(d,p) computational levels. Calculations taking into account all minima (T = 298.16 and 0 K) for every configuration

	B3LYP				M06-2X			
	D-Ribose		2-Deoxy-D-ribose		D-Ribose		2-Deoxy-D-ribose	
Structure	r.t.[b]	0 K	r.t.[b]	0 K	r.t.[b]	0 K	r.t.[b]	0 K
Open-chain	8.2	0.3	20.4	0.5	0.0	0.0	0.0	0.0
α-Furanose	3.4	1.5	6.2	2.4	0.2	0.1	0.8	0.3
β-Furanose	0.6	0.2	1.2	0.4	0.0	0.0	0.1	0.0
α-Pyranose	33.5	39.0	58.4	87.4	45.0	40.0	88.2	93.2
β-Pyranose	54.3	59.0	13.8	9.3	54.8	59.9	10.9	6.5

[a] $K = -RT \ln \Delta E_0$, where K is the population relationship, R the ideal gas constant, T the temperature and ΔE_0 the relative energy. [b] r.t. means 'room temperature'. T = 298.16 K.

In 2-deoxy-D-ribose, drastic differences are seen: (i) the significant population of open-chain 2-deoxy-D-ribose at room temperature is practically zero at 0 K; (ii) the β-pyranose form decreases in population; and (iii) there is a large gain of population for the α-pyranose form with the 87.4% of the total. In this case, the β/α ratio in pyranose forms decreases. In view of these results, it is clearly noted that the entropy factor in the B3LYP calculations becomes important especially for the open-chain forms in D-ribose and 2-deoxy-D-ribose. As can be seen in Table 2, open-chain forms at 0 K quantified a considerable percentage in D-ribose, and more prominently, in 2-deoxy-D-ribose, even exceeding the β-pyranose population.

Based on the M06-2X results, there is a clear relationship between the anomeric effect and the ring configuration in the pyranose forms of 2-deoxy-D-ribose. So, the hydroxyl group on C1, that is, attached to the anomeric carbon atom, presents *axial* disposition in their most stable minima. $^4C_1$ and $^1C_4$ ring conformations exhibit this disposition in the α- and β-pyranoses, respectively. The first *equatorial* disposition appears at 10.05 kJ mol^{-1} for α-2-deoxy-D-ribopyranose and at 5.84 kJ mol^{-1} for β-2-deoxy-D-ribopyranose. This observation is common in β-D-ribopyranose, however, in α-D-ribopyranose, the *equatorial* disposition of the hydroxyl group attached to C1 is preferred in the most stable minima.

In the comparison of our results for D-ribose with those obtained by Cocinero and co-workers,[18] some points should be highlighted: (i) our full exploration of the conformational landscape offers a higher number of stable structures; (ii) our relative ratios for β/α-pyranose are 1.6 : 1 (B3LYP) and 1.2 : 1 (M06-2X) at room temperature and 1.5 : 1 for both functionals at 0 K, which coincide with the Cocinero's DFT results; and (iii) however, in the B3LYP results of Cocinero *et al.* there is practically no population for open-chain and furanose forms (less than 1%), while in our case, this population is 12.2% at room temperature and 2.0% at 0 K.

2. Intramolecular weak interactions

In this section, three kinds of weak interactions will be commented: classical hydrogen bonds (HBs) between two hydroxyl groups (or even between one hydroxyl group and the aldehyde moiety in the open-chain forms), HB between one hydroxyl group as an HB acceptor and a CH as a donor (CH···O),[43,44] and O···C interactions.[42,45] Also, in the full exploration of the weak interactions present in all minima, a total of 19 bond paths which link two hydrogen atoms (H···H bonds) have been found.[46]

For this purpose, two methodologies were used: from the topological AIM approach, the presence/absence of an interatomic BCP with low values of the electron density and its Laplacian greater than zero determines the existence/non-existence of weak interactions, and from the NBO orbital approach, a numerical value is obtained for the stabilization interaction of the charge transfer between the involved orbitals.

Focusing our attention on the classical HB, these interactions have been classified as 1–2, 1–3, 1–4 and 1–5 type based on the number of C–C bonds (1, 2, 3, and 4 respectively) which separate the two interacting moieties. The number of total classical HBs in

all the unique minima obtained at the M06-2X/6-311++G(d,p) computational level is 1529, of which 457 are of 1–2 type, 761 are of 1–3 type, 264 are of 1–4 type and 47 are of 1–5 type. All these types of interactions are present in linear and cyclic configurations, except the 1–5 type which is only observed in the linear forms, when the two interacting groups are the hydroxyl group on C5 and the aldehyde moiety. The number of 1–2 type interactions in linear forms is large and they usually take place between the hydroxyl group on C2 and the aldehyde moiety due to the higher flexibility of this last group with respect to the two neighbor hydroxyl ones. These last interactions are less present in cyclic forms because of the geometrical restrictions.

Concerning the potential role of the ring oxygen atom as an HB acceptor, it is not present in any of the furanose minima but it is in some of the pyranose ones, particularly in minima with energy higher than 5 kJ mol^{-1}. These results are in agreement with a previous report on the D-erythrose and D-threose.[22]

Based on the AIM criteria, the classical HBs have distances which range between 1.80 and 2.40 Å, 1.90 and 2.47 Å, and 1.84 and 2.35 Å for open-chain, furanose and pyranose forms, respectively. Also, the electronic density and its Laplacian at BCP for all minima range between 0.036 and 0.010 au, and 0.035 and 0.128 au, which are in agreement with the intervals proposed by Koch and Popelier[47] to characterize HBs based on electron density descriptors. As can be seen in Fig. 6, the range of distances in 1–2 type interactions is much smaller than in the rest of the cases, the largest being found in the 1–4 type interactions. Fig. 6(a), (b) and (c), provides important information with regard to the geometrical and electronic nature of the

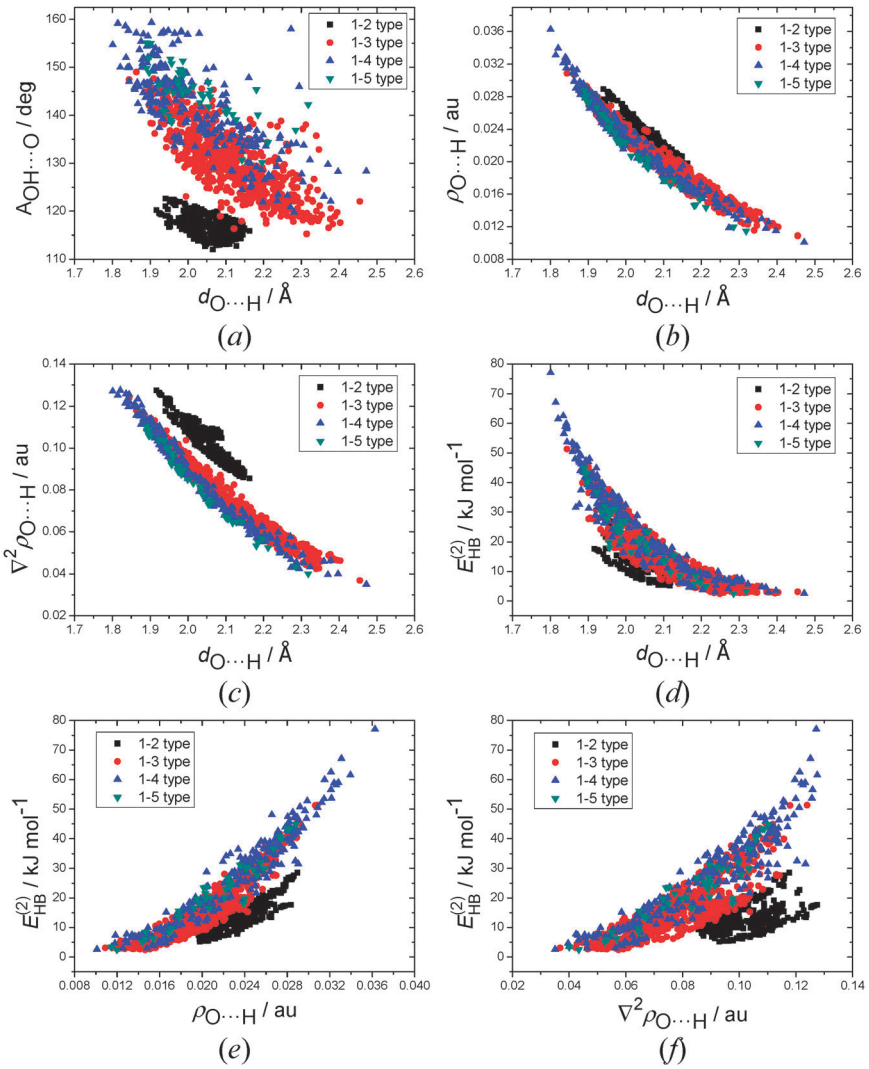

Fig. 6 (a) O···HO geometrical angle in degrees *versus* O···H distance in Å; (b) electron density at BCP in au *versus* O···H distance in Å; (c) Laplacian at BCP in au *versus* O···H distance in Å; (d) second-order orbital interaction energy in kJ mol^{-1} *versus* O···H distance in Å; (e) second-order orbital interaction energy in kJ mol^{-1} *versus* electron density at BCP in au; and (f) second-order orbital interaction energy in kJ mol^{-1} *versus* Laplacian at BCP in au, for the hydroxyl–hydroxyl and hydroxyl–aldehyde HB present in all minima of 2-deoxy-D-ribose and D-ribose (open-chain, furanose and pyranose forms). Black squares refer to 1–2, red circles to 1–3, blue triangles to 1–4 and green inverted triangles to 1–5 type interactions. All data are calculated at the M06-2X/6-311++G(d,p) computational level.

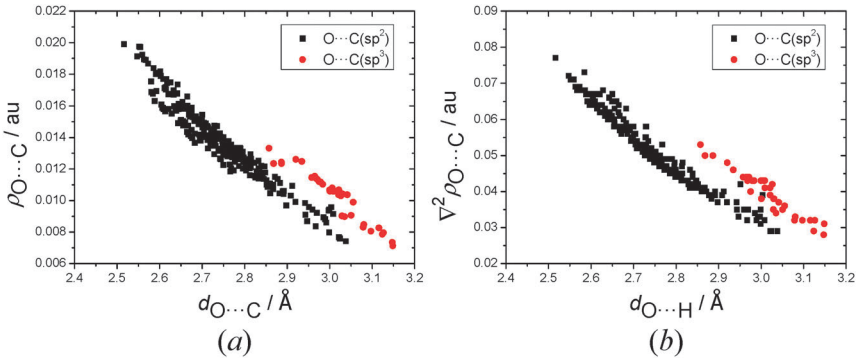

Fig. 7 (a) Electron density at BCP in au *versus* O···C distance in Å; (b) Laplacian at BCP in au *versus* O···C distance in Å. There are two types of weak interactions, on basis of the nature of the carbon atom, *i.e.*, sp^2 or sp^3. All data are calculated at the M06-2X/6-311++G(d,p) computational level.

classical HB that we are discussing here. Thus, the representation (a) shows clearly that the four type interactions taking place in 2-deoxy-D-ribose and D-ribose are clustered according to the number of C–C bonds which separate the interacting hydroxyl groups, paying special attention to the geometrical restrictions that 1–2 type exhibit with respect to the rest ones with regard to the size of the pseudo-ring (OH ··· O angle *versus* O···H distance). Furthermore, representations (b) and (c) show again this clustering, especially when the Laplacian at BCP is studied *versus* the interatomic distance with a clear separation of the 1–2 type interactions. In these two cases, very good exponential correlations are obtained, of 0.86, 0.96, 0.98 and 0.99 for the electronic density, and 0.82, 0.97, 0.98 and 0.99 for its Laplacian for 1–2, 1–3, 1–4 and 1–5 types, respectively. The values of the electron density descriptors become smaller as the size of the pseudo-ring increases.[48] These correlations are in agreement with previous reports on intramolecular interactions.[49,50]

Based on the NBO methodology, the classical HB is supported by an orbital interaction between the lone pair(s), *n*, of the hydroxylic or the carbonyl oxygen atom and the σ* orbital of the covalent O–H or C(sp^2)–H bond. Fig. 6(d) presents the values of the second order interaction energy for the $n \rightarrow \sigma^*$ orbital charge transfer *versus* the interatomic O···H distance, for those cases with an energy exceeding the 0.5 kcal mol^{-1} cut-off. An exponential behavior of the curves is observed. Additionally, Fig. 6(e) and (f) represents the relationship between $E^{(2)}$ and the topological variables ρ and its Laplacian at the BCP, with an exponential dependence too. In these three cases, there is a clear separation between the 1–2 type interactions and the others.

There are two types of O···C interactions, when the carbon atom has sp^2 or sp^3 hybridization. Both cases are clearly separated in terms of the electron density and its Laplacian at BCP *versus* the interatomic distance. Additionally, the distance intervals in which they take place are significantly larger: O···C(sp^2) bonds range between 2.5 and 3.1 Å and O···C(sp^3) ones between 2.8 and 3.2 Å (Fig. 7). A total of 240 O···C(sp^2) bonds have been computed, which are present only in linear forms, the O···C=O angles ranging between 85° and 120°. Minima ninth (E_{rel} = 3.9 kJ mol^{-1}) and fourth (E_{rel} = 5.0 kJ mol^{-1}) in open-chain D-ribose and 2-deoxy-D-ribose respectively exhibit this kind of interaction, similarly described in the conformational study of the salicylic acid,[42] in some of the acyclic forms of the aldotetroses D-erythrose and D-threose[22] and other similar interactions.[51–53] Only 38 O···C(sp^3) interactions are present in the open-chain forms of both monosaccharides and in the α- and β-furanose configurations of 2-deoxy-D-ribose. With the exception of the β-2-deoxy-D-ribofuranose, the O···C(sp^3) interactions are encountered only in high-energetic minima. These interactions can be divided into three groups based on the atom attached to the C one (O···C–X, X = O, H and C). Linear O···C(sp^3)–O interactions, similar to those described by Mani and Arunan,[45] have been found in all these structures with the exception of β-2-deoxy-D-ribofuranose; in which linear O···C(sp^3)–H interactions have been encountered with O···C–H angle values ranging between 165° and 170° and with long interatomic distances (between 3.02 and 3.06 Å). O···C(sp^3)–H interactions have been also found in open-chain D-ribose and α-2-deoxy-D-ribofuranose. Finally, similar O···C(sp^3)–C interactions are present only in open-chain forms.

Finally, the ESI† gathers the topological properties and the interatomic distances of other type of interactions found in all the sets of minima: C(sp^2)···HC, H···H and O···HC bonds.

Conclusions

In this work we report a full exploration of the conformational landscape in the gas phase for the D-ribose and 2-deoxy-D-ribose monosaccharides in their open-chain, furanose (α- and β-) and pyranose (α- and β-) configurations. Up to 954 and 668 stable structures have been obtained for D-ribose and 2-deoxy-D-ribose at the two DFT computational levels used. Of these, up to 35 and 22 structures have energies less than 5 kJ mol^{-1}. In both open-chain sugars, the most stable structure has *tt* conformation and the first compact structure appears in the sixth (*gg*, E_{rel} = 3.2 kJ mol^{-1}) and second (*gg′*, E_{rel} = 2.8 kJ mol^{-1}) energy ranking positions for D-ribose and 2-deoxy-D-ribose, respectively. The most stable structures in furanose forms present ^4E (α-2-deoxy-D-ribofuranose and β-D-ribofuranose), $^2T_1$ (β-2-deoxy-D-ribofuranose) and E_2 (α-D-ribofuranose) ring conformations. In the case of pyranose forms, only $^1C_4$ and $^4C_1$ ones have been found in the most stable minima for both molecules.

Table 3 Boltzmann populations[a] summary in percentage for D-ribose and 2-deoxy-D-ribose

	Our M06-2X results				Other results				
	D-Ribose		2-Deoxy-D-ribose		D-Ribose				
Structure	r.t.[b]	0 K	r.t.[b]	0 K	Solid[16]	Solution 0 °C[17]	Solution 90 °C[17]	Gas[c] theor.[18]	Gas exp.[18]
Open-chain	0.0	0.0	0.0	0.0	—	—	—	0.00	—
α-Furanose	0.2	0.1	0.8	0.3	—	5	22	0.04	—
β-Furanose	0.0	0.0	0.1	0.0	—	10	18	0.35	—
α-Pyranose	45.0	40.0	88.2	93.2	33.3–25.0	42	30	35.8	32.5
β-Pyranose	54.8	59.9	10.9	6.5	66.7–75.0	43	30	63.8	65.4

[a] $K = -RT \ln \Delta E_0$, where K is the population relationship, R the ideal gas constant, T the temperature and ΔE_0 the relative energy. [b] r.t. means 'room temperature'. T = 298.16 K. [c] MP2 calculations.

For D-ribose, pyranose forms (α- and β-) are the most populated according to both B3LYP and M06-2X functionals, the β-diastereoisomer being more populated. M06-2X results provide practically no population for open-chain and furanose forms, while for B3LYP, their sum reaches 12%. For 2-deoxy-D-ribose, both functionals yield different results, especially concerning the open-chain populations: 20% in B3LYP and a negligible percentage in M06-2X. In both cases, a majority of α-pyranose form has been obtained but with different values of 58 and 88%, respectively. The β/α ratio in pyranose forms present different results for both functionals: for M06-2X increases in D-ribose and decreases in 2-deoxy-D-ribose at 0 K with respect to the room temperature results are observed, the opposite case occurring in B3LYP. Table 3 gathers the Boltzmann populations summary in percentage for D-ribose and 2-deoxy-D-ribose, *i.e.*, the results obtained in this study and those collected from the literature and which have been exposed in the Introduction and Discussion parts.

Intramolecular hydrogen bonds (HBs) have been characterized by AIM and NBO methodologies. Four types of O–H···O interactions have been differentiated: 1–2, 1–3, 1–4 and 1–5, in which the second digit refers to the number of carbon skeleton atoms which separate the interacting acceptor–donor HB centers. Good correlations between the electronic density and its Laplacian at BCP *versus* the interatomic distances have been obtained. Also, exponential trends have been observed between $E^{(2)}$ NBO energies and these variables, ρ and $\nabla^2\rho$, noting the relationship between variables of different nature, that is, between topological (AIM) and orbital (NBO) approaches.

Finally, O···C interactions have been described, highlighting their abundant presence in the open-chain sugars, O···C(sp^2), and their presence in the most stable minima of β-2-deoxy-D-ribofuranose, O···C(sp^3).

Acknowledgements

LMA thanks MICINN for a PhD grant (No. BES-2010-031225). MMQM thanks the University of Jaén for a predoctoral fellowship. This work has been supported by MINECO (Project No. CTQ2012-35513-C02-02), the Comunidad Autónoma de Madrid (Project MADRISOLAR2, ref. S2009/PPQ-1533) and the Junta de Andalucía (project P08-FQM-04096). Gratitude is also due to the University of Jaén for continuing financial support and to the CESGA and CTI (C.S.I.C.) for allocation of computer time.

References

1 M. Sinnott, *Carbohydrate Chemistry and Biochemistry, Structure and Mechanism*, RSC Publishing, Royal Society of Chemistry, London, UK, 2013.
2 P. H. Seeberger and D. B. Werz, *Nature*, 2007, **446**, 1046–1051.
3 M. P. Freitas, *Org. Biomol. Chem.*, 2013, **11**, 2885–2890.
4 C. Wang, Z. Chen, W. Wu and Y. Mo, *Chem.–Eur. J.*, 2013, **19**, 1436–1444.
5 A. Ardá, M. Á. Berbís, P. Blasco, A. Canales, F. J. Cañada, M. C. Fernández-Alonso, F. Marcelo and J. Jiménez-Barbero, *Carbohydr. Chem.*, 2009, **35**, 333–355.
6 E. J. Cocinero, A. Lesarri, P. Écija, Á. Cimas, B. G. Davis, F. J. Basterretxea, J. A. Fernández and F. Castaño, *J. Am. Chem. Soc.*, 2013, **135**, 2845–2852.
7 H. A. Taha, M. R. Richards and T. L. Lowary, *Chem. Rev.*, 2012, **113**, 1851–1876.
8 E. Herbst and E. F. van Dishoeck, *Annu. Rev. Astron. Astrophys.*, 2009, **47**, 427–480.
9 P. Ehrenfreund and J. Cami, *Cold Spring Harb. Perspect. Biol.*, 2010, **2**, a002097.
10 J. M. Hollis, P. R. Jewell, F. J. Lovas, A. Remijan and H. Møllendal, *Astrophys. J.*, 2004, **610**, L21–L24.
11 D. T. Halfen, A. J. Apponi, N. Woolf, R. Polt and L. M. Ziurys, *Astrophys. J.*, 2006, **639**, 237–245.
12 J. M. Hollis, F. J. Lovas and P. R. Jewell, *Astrophys. J.*, 2000, **540**, L107–L110.
13 J. M. Hollis, S. N. Vogel, L. E. Snyder, P. R. Jewell and F. J. Lovas, *Astrophys. J.*, 2001, **554**, L81–L85.
14 J. M. Hollis, P. R. Jewell, F. J. Lovas and A. Remijan, *Astrophys. J.*, 2004, **613**, L45–L48.
15 G. Cooper, N. Kimmich, W. Belisle, J. Sarinana, K. Brabham and L. Garrel, *Nature*, 2001, **414**, 879–883.
16 D. Šišak, L. B. McCusker, G. Zandomeneghi, B. H. Meier, D. Bläser, R. Boese, W. Bernd Schweizer, R. Gilmour and J. D. Dunitz, *Angew. Chem., Int. Ed.*, 2010, **49**, 4503–4505.
17 R. U. Lemieux, L. Anderson and A. H. Conner, *Carbohydr. Res.*, 1971, **20**, 59–72.

18 E. J. Cocinero, A. Lesarri, P. Écija, F. J. Basterretxea, J.-U. Grabow, J. A. Fernández and F. Castaño, *Angew. Chem., Int. Ed.*, 2012, **51**, 3119–3124.
19 A. D. Becke, *J. Chem. Phys.*, 1993, **98**, 5648–5652.
20 C. T. Lee, W. T. Yang and R. G. Parr, *Phys. Rev. B Condens. Matter Mater. Phys.*, 1988, **37**, 785–789.
21 M. J. Frisch, J. A. Pople and J. S. Binkley, *J. Chem. Phys.*, 1984, **80**, 3265–3269.
22 L. M. Azofra, I. Alkorta, J. Elguero and P. L. A. Popelier, *Carbohydr. Res.*, 2012, **358**, 96–105.
23 Y. Zhao and D. Truhlar, *Theor. Chem. Acc.*, 2008, **120**, 215–241.
24 J. R. A. Moreno, F. P. Ureña and J. J. L. González, *Tetrahedron: Asymmetry*, 2012, **23**, 780–788.
25 J. R. A. Moreno, M. d. M. Q. Moreno, F. P. Ureña and J. J. L. González, *Tetrahedron: Asymmetry*, 2012, **23**, 1084–1092.
26 S. N. Steinmann, C. Piemontesi, A. Delachat and C. Corminboeuf, *J. Chem. Theory Comput.*, 2012, **8**, 1629–1640.
27 M. J. Frisch, G. W. Trucks, H. B. Schlegel, G. E. Scuseria, M. A. Robb, J. R. Cheeseman, G. Scalmani, V. Barone, B. Mennucci, G. A. Petersson, H. Nakatsuji, M. Caricato, X. Li, H. P. Hratchian, A. F. Izmaylov, J. Bloino, G. Zheng, J. L. Sonnenberg, M. Hada, M. Ehara, K. Toyota, R. Fukuda, J. Hasegawa, M. Ishida, T. Nakajima, Y. Honda, O. Kitao, H. Nakai, T. Vreven, J. A. Montgomery Jr., J. E. Peralta, F. Ogliaro, M. Bearpark, J. J. Heyd, E. Brothers, K. N. Kudin, V. N. Staroverov, R. Kobayashi, J. Normand, K. Raghavachari, A. Rendell, J. C. Burant, S. S. Iyengar, J. Tomasi, M. Cossi, N. Rega, N. J. Millam, M. Klene, J. E. Knox, J. B. Cross, V. Bakken, C. Adamo, J. Jaramillo, R. Gomperts, R. E. Stratmann, O. Yazyev, A. J. Austin, R. Cammi, C. Pomelli, J. W. Ochterski, R. L. Martin, K. Morokuma, V. G. Zakrzewski, G. A. Voth, P. Salvador, J. J. Dannenberg, S. Dapprich, A. D. Daniels, Ö. Farkas, J. B. Foresman, J. V. Ortiz, J. Cioslowski and D. J. Fox, *Gaussian, Inc.*, Wallingford CT, 2009.
28 D. Cremer and J. A. Pople, *J. Am. Chem. Soc.*, 1975, **97**, 1354–1358.
29 C. Altona and M. Sundaralingam, *J. Am. Chem. Soc.*, 1972, **94**, 8205–8212.
30 D. Cremer, *J. Phys. Chem.*, 1990, **94**, 5502–5509.
31 R. F. W. Bader, *Atoms in Molecules: A Quantum Theory*, Clarendon Press, Oxford, 1990.
32 P. L. A. Popelier, *Atoms In Molecules. An introduction*, Prentice Hall, Harlow, England, 2000.
33 P. L. A. Popelier, *Chem. Phys. Lett.*, 1994, **228**, 160–164.
34 P. L. A. Popelier, *MORPHY 0.2 ed.*, 1999.
35 M. Rafat and P. L. A. Popelier, *J. Comput. Chem.*, 2007, **28**, 2602–2617.
36 T. A. Keith, *AIMAll, version 13.11.04*, 2013, http:\\aim.tkgristmill.com.
37 I. Rozas, I. Alkorta and J. Elguero, *J. Am. Chem. Soc.*, 2000, **122**, 11154–11161.
38 D. Cremer, *Croat. Chem. Acta*, 1984, **57**, 1259.
39 F. Weinhold and C. R. Landis, *Valency and Bonding. A Natural Bond Orbital Donor-Acceptor Perspective*, Cambridge Press, Cambridge, 2005.
40 E. D. Glendening, A. E. Reed, J. E. Carpenter and F. Weinhold.
41 L. M. Azofra, I. Alkorta and J. Elguero, *Carbohydr. Res.*, 2013, **372**, 1–8.
42 A. Choudhary, K. J. Kamer and R. T. Raines, *J. Org. Chem.*, 2011, **76**, 7933–7937.
43 T. Steiner and W. Saenger, *J. Am. Chem. Soc.*, 1992, **114**, 10146–10154.
44 T. Steiner and W. Saenger, *J. Am. Chem. Soc.*, 1993, **115**, 4540–4547.
45 D. Mani and E. Arunan, *Phys. Chem. Chem. Phys.*, 2013, **15**, 14377–14383.
46 C. F. Matta, J. Hernández-Trujillo, T.-H. Tang and R. F. W. Bader, *Chem.–Eur. J.*, 2003, **9**, 1950–1951.
47 U. Koch and P. L. A. Popelier, *J. Phys. Chem.*, 1995, **99**, 9747–9754.
48 M. Solimannejad, S. Massahi and I. Alkorta, *Int. J. Quantum Chem.*, 2011, **111**, 3057–3069.
49 I. Alkorta, K. Zborowski, J. Elguero and M. Solimannejad, *J. Phys. Chem. A*, 2006, **110**, 10279–10286.
50 I. Mata, I. Alkorta, E. Molins and E. Espinosa, *Chem.–Eur. J.*, 2010, **16**, 2442–2452.
51 I. Alkorta, F. Blanco, J. Elguero, J. A. Dobado, S. M. Ferrer and I. Vidal, *J. Phys. Chem. A*, 2009, **113**, 8387–8393.
52 I. Alkorta, I. Rozas and J. Elguero, *J. Org. Chem.*, 1997, **62**, 4687–4691.
53 I. Alkorta, I. Rozas and J. Elguero, *J. Am. Chem. Soc.*, 2002, **124**, 8593–8598.

